[11] Andrews, J. S., "The Effects of Transonic Buffeting on a Hammerhead Shaped Payload," *AIAA Symposium on Structural Dynamics and Aeroelasticity*, Boston, Mass., Aug. 30–Sept. 1, 1965.

[12] Bisplinghoff, R. L., Ashley, H., and Halfman, R. L., *Aeroelasticity*, Addison-Wesley Publishing Co., Reading, Mass., 1965

[13] Goldberg, A. P. and Wood, J. D., "Dynamic Loads on the Atlas Able 5 During Transonic and Low Supersonic Speeds," STL/TM 60-0000-19075, Aug. 22, 1960, Space Technology Laboratories, Los Angeles, Calif.

[14] Houbolt, J. C., "Structural Response of Re-Entry Vehicles to Boundary Layer Noise," GE-RESD, TIS 65SD223, March, 1965, General Electric, Philadelphia, Pa.

[15] Houbolt, J. C., "On the Estimation of Pressure Fluctuations in Boundary Layers and Wakes," GE-RESD, TIS 66SD296, Aug., 1966, General Electric, Philadelphia, Pa.

[16] Studerus, C. J. and Dienna, E. A., "Viscous Interaction Zero Angle of Attack Drag (VIZAAD) Program," GE, TIS 64SD292, Nov. 1964, General Electric, Philadelphia, Pa.

[17] Martellucci, A. and Rie, H., "Effects of Mass Addition on Viscous Flow Parameters," SAMSO TR-71-60, also GE TIS 71SD205, March, 1971, General Electric, Philadelphia, Pa.

[18] Rosenbaum, H. and Margolis, D. P., "Pressure Fluctuations Beneath an Incompressible Turbulent Boundary Layer with Mass Addition," *The Physics of Fluids*, Vol. 10, No. 6, June 1967.

DECEMBER 1973 J. SPACECRAFT VOL. 10, NO. 12

Application of Sequential Filtering to Estimation of the Interplanetary Orbit of Mariner 9

KENNETH H. ROURKE* AND JAMES F. JORDAN†
Jet Propulsion Laboratory, Pasadena, Calif.

This paper presents the results of the application of sequential filtering to the determination of the interplanetary orbit of the Mariner 9 spacecraft. The technique is a specific extension of the Kalman filter. The special problems associated with applying this technique are discussed and the particular algorithmic implementations are outlined. The method is compared against the weighted least squares filters of conventional application. The results reveal that relatively simple sequential filter configurations yield solutions superior to those of the conventional method when applied to radio measurements of Mariner 9.

Nomenclature

X = spacecraft position vector
V = spacecraft velocity vector
u = spacecraft nongravitational accelerations
Z = $F(X, V, t)$, observational data vector
ε = observation error
x = $[(X - X_{\text{nominal}})^T, (V - V_{\text{nominal}})^T]^T$ position and velocity, i.e., "state" deviation vector
z = $Z - Z_{\text{nominal}}$, observational data deviation vector
$(\cdot)^T$ = transpose operation
T_k = filter batch break times
x_k = $x(T_k)$, discretized state
$\Phi(T_{k+1}, T_k)$ = $\partial x_{k+1}/\partial x_k$, state transition matrix
$\Gamma(T_{k+1}, T_k)$ = $\partial x_{k+1}/\partial u_k$, acceleration transition matrix
z_k = $[z^T(t_1), \ldots, z(t_{n_k})]^T$, $T_k \leq t_1, \ldots, t_{n_k} \leq T_{k+1}$, data vector for data in batch $[T_k, T_{k+1}]$
A_k = $\partial z_k/\partial x_k$, state data partial derivatives
B_k = $\partial z_k/\partial u_k$, acceleration data partial derivatives
Δv = velocity increment vector
$B \cdot T$ = component of spacecraft asymptotic miss vector in the ecliptic plane
$B \cdot R$ = component of spacecraft asymptotic miss vector normal to the ecliptic plane
Δa = spacecraft acceleration correction model

Presented as Paper 72-906 at the AIAA/AAS Astrodynamics Conference, Palo Alto, Calif., September 11–12, 1972; submitted October 30, 1972; revision received July 27, 1973. This paper presents one phase of research carried out at the Jet Propulsion Laboratory, California Institute of Technology, under NASA Contract NAS7-100.

Index categories: Spacecraft Navigation, Guidance, and Flight-Path Control Systems; Spacecraft Tracking; Navigation, Control, and Guidance Theory.

* Senior Research Engineer, Interplanetary Orbit Determination Group.

† Group Supervisor, Satellite Orbit Determination and Planetology Group.

Introduction

OVER the past decade the navigation of the United States' interplanetary spacecraft has relied almost exclusively on Earth based radio orbit determination. Radio orbit determination accuracies have improved by more than an order of magnitude during the last 10 years; from the errors of 1300 km encountered during the Mariner 2 mission to Venus in 1962, to the 50-km errors experienced in navigating Mariner 9 to Mars in 1971.

These performance improvements have been brought about by the concurrent improvements made in the quality of the basic radio orbit determination data types, range and range rate, now accurate to 15m and 1 mm/sec, respectively.

The remaining errors which affect the accuracy of interplanetary orbit determination are uncertainties in the measurement and spacecraft dynamics models which produce range change errors when matching passes of tracking data to estimated orbits.

A major error arises from the diurnal range change due to uncertainties in the tracking stations' Earth-fixed coordinates. Indeed, uncertainties in the locations of the tracking stations are the principal limitation to determination of spacecraft geocentric angles from single passes of tracking data. Current station location errors of 3–7 m, which include the equivalent effects of both charged and neutral particles on the radio signal, can produce orbit estimate errors of approximately 100–200 km at typical Earth-Mars encounter distances.[1]

The principal dynamic model errors arise from small forces due to spacecraft attitude control system and propulsion system leaks, as well as errors in the spacecraft solar radiation force model. The direct effect of the spacecraft acceleration errors on the physical motion of the spacecraft is usually small; although acceleration errors can severely limit the capability of solving for the orbit using Earth based radio measurements. Indeed, spacecraft movements of approximately 6 m over 12 hr, which are comparable to station location errors, can arise from spacecraft accelerations on the order of 10^{-11} km/sec^2.

Central to the data processing software is the data filter, the basic algorithm used to produce accurate orbit estimates from redundant navigational observations. The filters that have been used in navigating the past interplanetary missions are fundamentally equivalent to the well-known least squares orbit determination methods developed by Gauss more than 100 years ago. These traditional methods have been retained despite the considerable theoretical and practical filter developments of the past decade. Theoretically antiquated, the least squares filter has, nevertheless, proved itself a simple yet accurate means for providing interplanetary orbit estimates. The favorable performance of the least squares techniques results largely from the extreme precision afforded by the dynamic models of interplanetary ballistic spacecraft motion. However, the increased demands on radio orbit determination have recently elevated the spacecraft dynamics errors to the status of a major error source.

This paper presents the results of an application of a batch-sequential filter to determining the interplanetary orbit of Mariner 9 from actual tracking data obtained during the approach phase, where the term batch-sequential filter refers to a particular extension of the Kalman filter described in the following. Mariner 9 provides a special opportunity for testing the batch-sequential filtering since, during the two months prior to Mars encounter, the spacecraft experienced a series of attitude control leaks, and the resulting small forces acting on the spacecraft were of sufficient magnitude to introduce sizable errors in particular orbit estimates. The objective of this paper is to demonstrate the effectiveness of the sequential filter to reduce orbit estimate sensitivities to small spacecraft forces by comparing the sequential and conventional estimates of the Mariner 9 interplanetary orbit.

The motivation for applying a batch-sequential filter to spacecraft tracking data lies in the fact that due to the random nature of the spacecraft acceleration errors, their effect—with proper data filtering—can be distinguished to some degree from the station location errors that so strongly affect the orbit estimates. Proper filtering can be expected to result from proper descriptions of the spacecraft dynamical errors, descriptions best provided by sequential orbit determination filtering techniques.

The Orbit Determination Data Filter

The specific filter algorithm adopted for this study has been selected to treat spacecraft acceleration errors. Although this is a limited point of view, it is adequate here. More general sequential filter development is covered in a multitude of sources (including Refs. 2–4).

Consider then a spacecraft with Cartesian position and velocity vectors X, V, respectively. The spacecraft motion is represented in terms of a system of differential equations:

$$\begin{aligned} \dot{X} &= V \\ \dot{V} &= G(X) + u(t) \qquad t \geq t_0 \\ X(t_0) &= X_0 \quad \text{and} \quad V(t_0) = V_0 \end{aligned} \tag{1}$$

where $G(X)$ represents gravitational accelerations and $u(t)$ represent spacecraft generated accelerations. The spacecraft's motion is observed via data equations

$$Z(t_i) = F(X,V,t_i(t_i) + \varepsilon) \qquad i = 1, \ldots, N \tag{2}$$

where $F(X,V,t)$ expresses observables, e.g., doppler and range data, in terms of the spacecraft "state." The $\varepsilon(t)$ represents data errors.

The problem in orbit determination is to estimate $x(t)$ given $z(t_i)$ for $t_i < t$, where $x(t)$ and $z(t_i)$ are deviations from a nominal state (position and velocity) history and data history.

If $u(t) \equiv 0$, or can be represented in terms of a limited number of parameters, then estimating $x(t)$ reduces to estimating x_0 and the u-parameters; a set of fixed quantities. This problem can be accomplished with conventional least squares or "batch" filtering algorithms. However, if $u(t)$ is too complex in structure to permit representation by a limited set of parameters, an alternate approach is required. Assume then that $u(t)$ is representable as a piecewise constant function; that is, for a sequence of break times $T_1, \ldots, T_M$, $u(t)$ satisfies

$$u(t) = u_k \quad \text{if} \quad T_k < t \leq T_{k+1} \qquad k = 1, \ldots, M$$

where $u_k (k = 1, \ldots, M)$ is a sequence of constant vectors. The linearized system can be then recast into a sequential form as follows:

$$x_{k+1} = \Phi(T_{k+1},T_k)x_k + \Gamma(T_{k+1},T_k)u_k \tag{3}$$

$$z_k = A_k x_k + B_k u_k + \varepsilon_k \tag{4}$$

where $x_k = x(T_k)$ and z_k is a vector which contains all data acquired between T_k and T_{k+1}. Φ, Γ, A and B are the appropriate state transition and data partial derivative matrices, respectively.

The linearized model expressed in Eqs. (3) and (4) is referred to as the batch sequential dynamic model. It provides a basis for applying any one of the numerous sequential filter formulations that arise from the basic Kalman algorithm.[2] The dynamical evolvement associated with spacecraft motion is typically slowly varying, with respect to data rate, implying that the batches just described can contain many data points. This is the prime motivation for the batch sequential form: allowing improved filter models without undergoing the decrease in data processing efficiency associated with a "point sequential" model, for which each batch break time is an observation time.[3] Algorithms for constructing an estimate of x_k given z_j $(j = 1, \ldots, k)$ require specification of a priori statistical properties of the initial state x_0, the data noise ε_k, and the process noise u_k. These specifications along with the batch structure, $T_1, \ldots, T_M$; can be considered as the design parameters for the sequential filter. There exist several options for treating the acceleration error sequence u_k. In this application, the u_k's are not directly estimated but are accounted for by uncorrelated velocity impulses in the dynamics. Thus

$$\Gamma(T_{k+1}, T_k)u_k = \begin{bmatrix} \Delta v \\ 0 \end{bmatrix} \tag{5}$$

and

$$B_k = 0 \tag{6}$$

It should be noted that a square root formulation[4] of the standard Kalman algorithm has been used to generate the results here. Estimation problems for interplanetary orbit determination based on Earth-based radio measurements are characteristically ill-conditioned, with covariance matrices whose eigenvalues range in magnitude by 10^{18} or 10^{20}. The square root formulation reduces the problem of ill-conditioning by reducing the spread of eigenvalues to less than 10^{10}.

The Filter Evaluation Test-Bed, Mariner 9

Mariner 9 was launched by NASA in May 1971. Continuous doppler and range data were acquired by DSN Stations until a few days before Martian encounter on Nov. 14, when the burn parameters for a large retro maneuver were loaded

into the spacecraft computer. The resulting maneuver, executed near the close approach, reduced the aerocentric velocity of the spacecraft such that the probe then orbited Mars with a period of 12 hr 37 min. Subsequent trim maneuvers reduced the orbital period to 11 hr 59 min.

All of the maneuvers which were executed on the Mariner 9 mission and on all previous Mariner missions have been planned and commanded on the basis of orbits determined from DSN tracking data. The large retro maneuver, performed at the Martian encounter of Mariner 9, was planned on the basis of a cruise orbit determined from 160 days of tracking. This long-arc of tracking data, covering almost the entire cruise phase of the mission, was available for determination of the spacecraft encounter orbit since a midcourse maneuver, originally scheduled 30 days before Martian encounter, was not performed. The target parameters from the estimated trajectory based on data to encounter minus 30 days were close enough to the desired target parameters to preclude the execution of the maneuver. If a pre-encounter midcourse maneuver had been performed, then the retro-maneuver at encounter would have been planned on the basis of an orbit estimated from data taken from the time of the midcourse until a few days before encounter, the "approach" portion of the cruise phase.

It is over just such an approach portion of the Mariner 9 orbit that the sequential filter has been tested. Results of the comparisons of the least squares or batch filter, and batch-sequential filter are given in terms of the asymptotic miss distance parameters in the plane which lies perpendicular to the aerocentric incoming asymptote of the spacecraft approach trajectory.[1] In that plane, the $B \cdot T$ coordinate lies in the ecliptic plane and the $B \cdot R$ coordinate lies perpendicular to the plane, thus unit vectors along the coordinates $B \cdot R$, $B \cdot T$, and the direction of the incoming aerocentric asymptote, form a right handed orthogonal system. Solutions are compared against the current best estimate of the target parameters, which have been determined from DSN data taken over the last few days of the cruise phase of the mission, which extends until 45 min before the terminal retro-maneuver. The current best values of the aerocentric miss coordinates and associated current uncertainties are given as

$$B \cdot T = 5588 \pm 10 \text{ km}, \qquad B \cdot R = 6085 \pm 10 \text{ km}$$

The high degree of accuracy of the current estimates results from the large degree of bending on the trajectory during the last few hours of data, enabling an accurate tie of the orbit estimate to the Martian center of mass.

The data span used in the filter evaluation test cases begins on Oct. 4, 06 hr, and ends on Nov. 6, 06 hr, which is approximately 8 days before encounter. The date Oct. 4 is chosen as a representative starting date (encounter—41 days) to relate to short arc orbit determination analysis for possible future Mars missions. The 8-day gap between the termination of data and the time of encounter allows time for a second midcourse maneuver, if required.

Throughout the testbed tracking span, two-way doppler and ranging data was obtained from tracking stations DSS 12, 14, 41, 51 and 62. The values of the observed data are, of course, dependent of the particular station's longitude and distance from the Earth's spin axis. Station location model values are obtained from processing data from the encounter portions of planetary missions. In this study two sets of station location values are used. The first set, which will be referred to as Set 1, was obtained from processing the Mars encounter data from Mariner 6 (Aug. 1969).[5] Since the solutions for the station locations are tied to the spacecraft position, and the spacecraft position is tied to the planet during the encounter phase of the mission, the errors in a particular station location solution set are correlated strongly with the errors in the currently employed ephemeris specification of the planet's position, at the time of the spacecraft encounter. Hence the station location values in Set 1 are effectively attached to the Martian position in the ephemeris at the Aug. 1969 epoch. The Martian position error in 1969, of course, need not coincide with the position error in Nov. 1971, hence the "equivalent" station location values which are best for Mariner 6 are not necessarily best for Mariner 9.

Table 1 Approximate station location values and differences between Mariner 9 and Mariner 6 solutions

Spin axis radius	Station location values (km, degrees east)	Set 2—Set 1 differences (meters)
DSS 12	5212.05	0.3
14	5203.99	0.3
41	5450.20	3.3
51	5742.94	−1.2
62	4860.82	2.7
Longitude		
DSS 12	243.19	−6.6
14	243.11	−7.0
41	136.89	−6.4
51	27.69	−6.5
62	355.63	−6.3

A second set of station location values, Set 2, was obtained by the authors from processing the last seven days of the Mariner 9 cruise data, i.e., the encounter phase. Approximate values of the DSN stations' spin radii and longitudes, as well as the differences between the Set 1 and Set 2 values are given in Table 1. The primary differences between the values of the two sets are the 7-m long differences between solutions. This difference indicates an approximate difference between the respective errors in the Earth-Mars relative ephemeris of Aug. 1969 and Nov. 1971 of 10^{-6} rad or 0.3 sec of arc in right ascension. It is difficult to say which of the two sets is more absolutely accurate, since the ephemeris errors at the two epochs are not known. However, the Set 2 values should be the more favorable set for testing filter behavior on Mariner 9.

The Mariner 9 spacecraft was attitude stabilized by a system which consists of sun and Canopus sensors, and coupled pitch, roll, and yaw gas jets. The jets are positioned near the ends of the solar panels as shown in Fig. 1. The pitch and yaw jets are aligned perpendicular to the direction from the jet to the center of the spacecraft, but the roll jets are canted by 21°. In Sept. 1971, the roll jet along the minus x axis began to develop occasional leaks. The leaks are believed to be caused by particles from a corroding valve stem that are caught in the valve during the closing of a normal firing and forcing it it remain slightly open. The leaks normally lasted several hours, or until the leak was

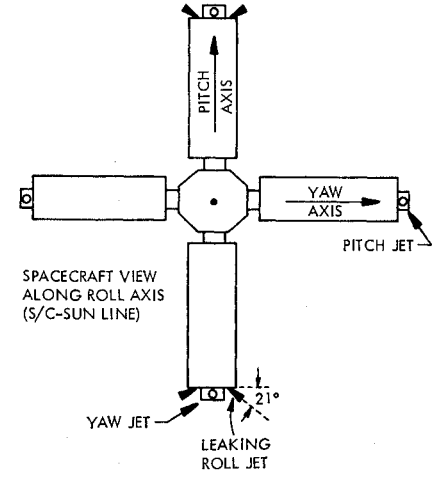

Fig. 1 Spacecraft view along roll axis (S/C–sun line).

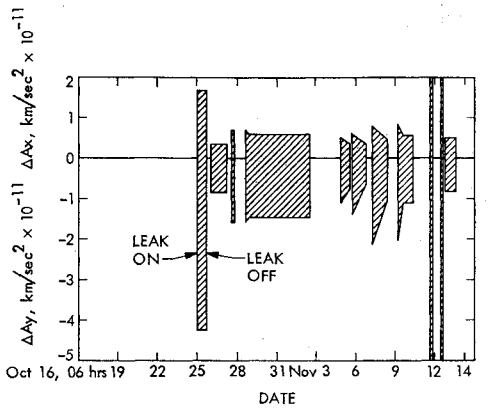

Fig. 2 Time history of accelerations due to gas leaks in the roll jet during the last month of cruise.

detected and the valve was cleared, and produced spacecraft accelerations with magnitudes above 10^{-11} km²/sec. Figure 2 illustrates the time history of the accelerations due to leaks in the roll valve over the last 40 days of the cruise phase of the mission. The values of the leak magnitudes and duration times were obtained from analysis of telemetered data of the light intensity time history of the spacecraft sun and Canopus sensors. The ability to obtain nonambiguous acceleration estimates from the telemetry data depended on the special center of mass and rotational inertia configuration that was characteristic of the MM'71 spacecraft. It should be noted that acceleration estimates of this type may not be generally available for future missions.

Solutions given in the following sections are obtained with the leak acceleration model of Fig. 2 both included and excluded from the spacecraft equations of motion. The cases in which the acceleration model is included correspond to a situation in which spacecraft engineering data is made available to the estimation process in near real-time. Cases in which the model is not included correspond to the situation where such data would not be available.

Batch Filter Results

Figure 3 illustrates the history of batch processing estimates of $B\cdot T$ and $B\cdot R$ as a function of the time of the last data point processed (in days past Oct. 4). The last solution, for day 41, includes data to Nov. 13, 18 hr. Station location Set 1 (from Mariner 6) is used in the observable model, and no acceleration model is included in the equations of motion. Hence this figure represents a conservative, realistic solution history.

Note that most of the movement of the solution, as more data are included in the processing, is in the $B\cdot R$ direction. The lack of orbit bending perpendicular to the ecliptic plane results in large sensitivities in $B\cdot R$ to the prominent errors, e.g., station location errors and acceleration errors. These sensitivities, which can fluctuate in magnitude with the addition of data in the span, are primarily responsible for the solution movement.

The large sensitivity in the $B\cdot R$ direction to model errors is also illustrated by Fig. 4, in which the aim plane parameters of the batch solutions of Fig. 4 are compared at the end of the approach phase (Nov. 6, 06 hr) to the parameters of the current best orbit estimate. A 1-σ dispersion ellipse for each value is also presented. The dimensions of the dispersion ellipse for the approach solution is primarily due to the ephemeris error associated station location uncertainties of 7 m (1σ) in longitude and 3 m (1σ) in spin axis value. These uncertainties map to a 200-km uncertainty in $B\cdot R$ and a 50-km uncertainty in $B\cdot T$, a four to one ratio in magnitude.

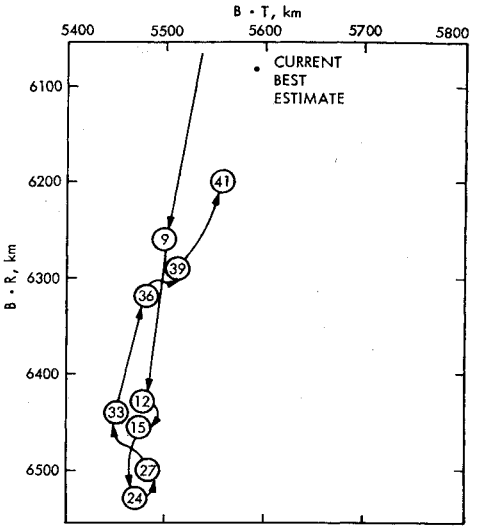

Fig. 3 Evolution of State estimate in the aim plane for the batch filter (set 1). Solutions labeled in days past Oct. 4.

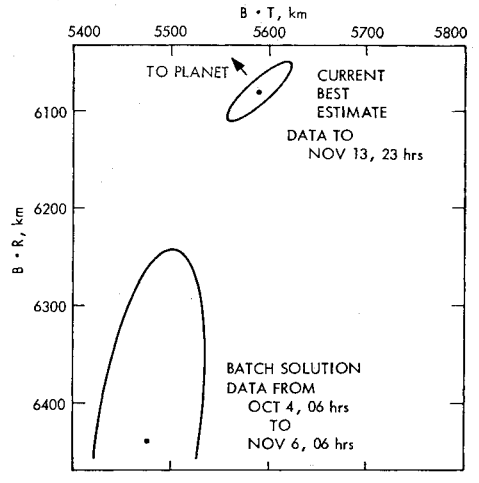

Fig. 4. Comparison of approach solution in the aim plane to current best estimate.

Since the salient solution behavior lies in the $B\cdot R$ direction, the remaining solution time histories presented in the paper are shown in terms of the behavior of $B\cdot R$ only. Figure 5 illustrates the time history of the $B\cdot R$ solution as a function of the time of the last processed data point for station location Set 1. The solution histories with and without the acceleration model of Fig. 2, are shown on the figure. Note that when the first leak occurs on Oct. 25, the solutions separate;

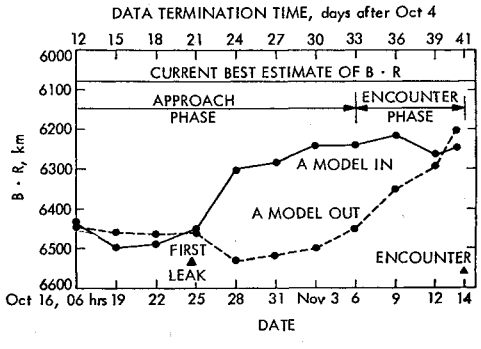

Fig. 5 Time history of $B\cdot R$ solution for batch estimate (set 1).

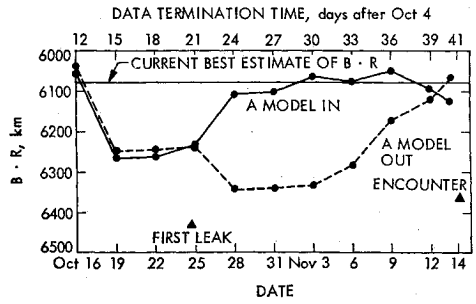

Fig. 6 Time history of $B \cdot R$ solution for batch estimate (set 2).

the solution without the Δa model tends toward a larger $B \cdot R$ error, while the solution containing the Δa model improves, and remains more accurate for the duration of the approach phase.

Figure 6 illustrates similar solution histories for station location Set 2 (Mariner 9). The solutions are shifted from the Set 1 solution in the minus $B \cdot R$ direction by approximately 200 km, which decreases the total error, and supports the conclusion that the Mariner 9 determined station location values (Set 2) are naturally more consistent with the ephemeris in 1971 than the Mariner 6 (Set 1) values. Again with Set 2, as with Set 1, inclusion of the engineering data determined Δa model results in more accurate solution after the commencement of the gas leaks. The salient characteristics of the batch solutions are that the aim plane parameters are extremely sensitive to both the values of the station locations and the random accelerations. Station location differences between Set 1 and Set 2 (7 m in longitude, and 3 m in spin axis) map to a 200-km difference in $B \cdot R$ for data taken to Nov. 6. The Δa-in, Δa-out difference in the equations of motion results in a $B \cdot R$ change of more than 150 km with either station location set. A batch solution with the Δa included and using Set 2, naturally is more accurate than the other solutions.

It should be noted, however, that the rapid solution improvement shortly after inclusion of the data in the vicinity of the first gas leak (Oct. 25) is not predictable from the sensitivity analysis performed to date. The time history of perturbations in the solution of $B \cdot R$, due to positive 7-m longitude and 3-m spin axis errors in all of the tracking stations, are given in Fig. 7. Although drop in sensitivity to spin axis on Oct. 16 can explain the rapid solution change in Fig. 6 on or around October 16, no such sensitivity change is evident in Fig. 7 near Oct. 25. Thus either the estimate is strongly sensitive to some model parameter other than the station location, or the value for the leak magnitude is strongly overmodelled. This problem has not yet been resolved, and is currently under study.

Sequential Filter Results

The sequential filter used for comparison processed successive batches whose durations are all equal to 36 hr. While processing each batch of data, the constraints imposed on the

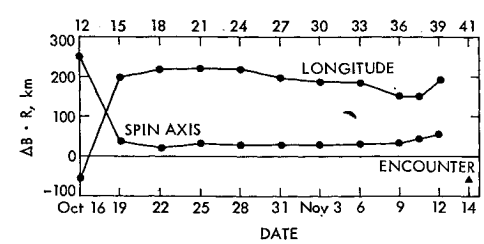

Fig. 7 Perturbation time history in $B \cdot R$ due to +7 m long and +3 m spin radius errors for the batch estimate.

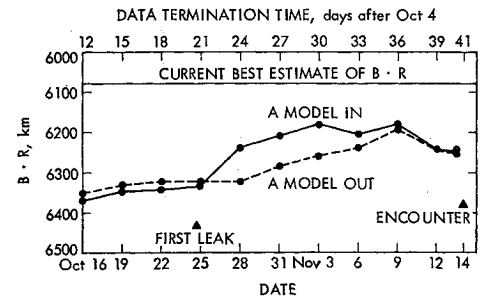

Fig. 8 Time history of $B \cdot R$ solution for 10^{-12} km/sec^2 sequential estimate (set 1).

state solution by the data in previous batches is loosened by the addition of instantaneous "process noise" on the velocities at the beginning of the batch. The magnitude of this degrading Δv is determined by integrating the values of an assumed constant acceleration over the 36 hr duration of the previous batch. Three magnitudes of assumed acceleration are considered in this paper, 10^{-12} km/sec^2, 10^{-11} km/sec^2 and 10^{-10} km/sec^2, and the values of instantaneous process noise are computed on the basis of these acceleration levels.

Figure 8 presents the $B \cdot R$ solution time history for the sequential processor constructed with Δv process noise corresponding to an acceleration error of 10^{-12} km/sec^2. Station location Set 1 is employed in the observable model, and curves for the Δa model in, and out, of the equations of motion are shown. Figure 9 illustrates the same sequential process or results for station location Set 2.

The differences between the Δa-in and Δa-out solutions are much smaller for the sequential processor than for the batch. The terminal difference in $B \cdot R$ for both station location sets is only a few kilometers. Thus the 10^{-12} km/sec^2 process noise decreases markedly the sensitivities of the solution to the use of gas leak model or absence of it. In addition, the solutions are brought closer to the current best estimate by the addition of process noise into the filter, and are indeed within 50 km for the case of the Mariner 9 station location values (Set 2).

The trend continues as the process noise is increased to correspond to accelerations of 10^{-11} km/sec^2, as shown in Figs. 10 and 11. The Δa model has little effect at all on the solution behavior, and solutions are more accurate than those with the smaller values of process noise.

The sensitivities of the sequential filter solutions to correlated station location errors are presented in Fig. 12 and are seen by comparison with Fig. 7 to have been decreased by the addition of 10^{-11} km/sec^2 process noise. These smaller sensitivities are consistent with the smaller absolute $B \cdot R$ errors occurring with the sequential processors.

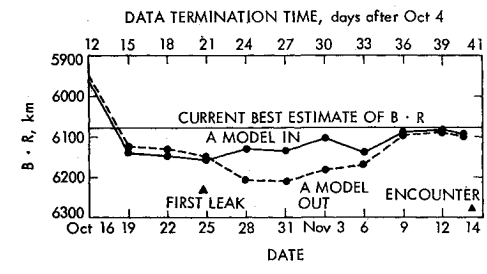

Fig. 9 Time history of $B \cdot R$ solution for 10^{-12} km/sec^2 sequential estimate (set 2).

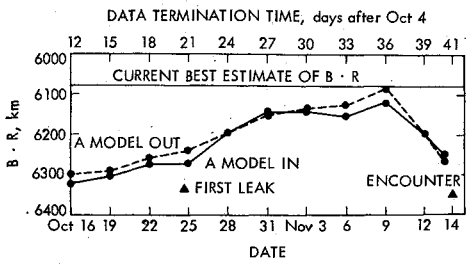

Fig. 10 Time history of $B \cdot R$ solution for 10^{-11} km/sec^2 sequential estimate (set 1).

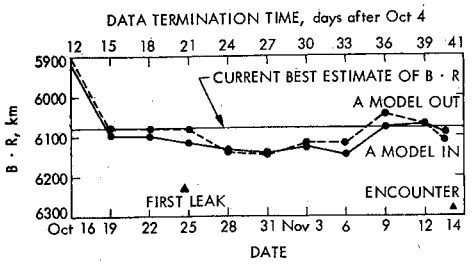

Fig. 11 Time history of $B \cdot R$ solution for 10^{-11} km/sec^2 sequential estimate (set 2).

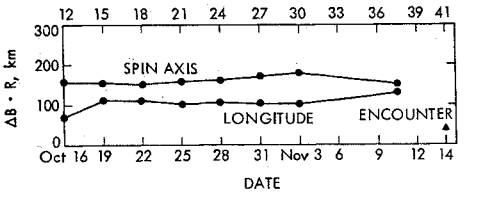

Fig. 12 Perturbation time history in $B \cdot R$ due to +7 km long. and +3 m spin radius errors for the 10^{-11} km/sec^2 sequential estimate

Summary

The results of this paper are summarized in Fig. 13 where the aim plane solutions at the end of the approach phase (Nov. 6) are shown for the batch (B) and sequential filters, (S_1, S_2, S_3) with respective process noise values representing acceleration errors of 10^{-12}, 10^{-11}, and 10^{-10} km/sec^2. Both Set 1 and Set 2 results are shown, with the Δa-in and Δa-out solutions, respectively represented with the head and tail of the arrows.

The following conclusions regarding the general behavior of the filter solutions can be drawn:

1) The solutions of the sequential filter are markedly improved over the batch solutions. The sensitivity of the Δa model is significantly diminished, indicating that the sequential filter does "filter out" the effects of random gas leaks.

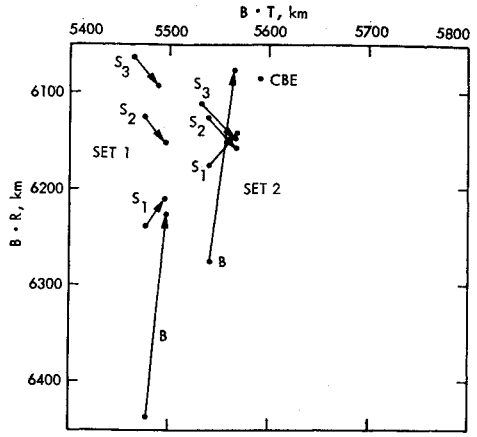

Fig. 13 Summary of approach solutions in the aim plane.

2) The sequential filter alleviates the effects of station location errors over the approach phase of Mariner 9. A comparison of the sensitivity analysis plots in Figs. 7 and 12 bears this out. It should be cautioned that this phenomenon is very possibly peculiar to Mariner 9 geometry and tracking patterns, and may not occur in the general case.

3) The sequential filters appear to perform better than the batch filter over a wide spread of process noise magnitude assumptions ($10^{-12} \rightarrow 10^{-10}$ km/sec^2) hence performance does not seem to be very sensitive to the users choice of process noise. It should also be noted that the times of the chosen batch separation points do not coincide with the times of gas leaks. Thus the filter behavior is probably not significantly degraded by the choice of any reasonable batch-break structure.

References

[1] Jordan, J. F., Madrid, G. A., and Pease, G. E., "The Effects of Major Error Sources on Planetary Spacecraft Navigation Accuracies," *Journal of Spacecraft and Rockets*, Vol. 9, No. 3, March 1972, pp. 196–204.

[2] Kalman, R. E., "A New Approach to Linear Filtering and Prediction Problems," *Transactions of ASME: Journal of Basic Engineering*, Vol. 82-D, 1960, pp. 35–45.

[3] Kaminski, P. G., Bryson, A. E., and Schmidt, S. F., "Discrete Square Root Filtering: A Survey of Current Techniques," *IEEE Transactions on Automatic Control*, Vol. AC-16, No. 6, Dec. 1971, pp. 727–736.

[4] Dyer, P. and McReynolds, S., "Extension of Square-Root Filtering to Include Process Noise," *Journal of Optimization Theory and Applications*, Vol. 3, No. 6, 1969, pp. 444–459.

[5] Mottinger, N. A. and Zielenbach, J. W., "Station Locations Provided for Mariner 9," TM 391-324, May 16, 1972, Jet Propulsion Lab., Pasadena, Calif.